Published online July 23, 2004

Nucleic Acids Research, 2004, Vol. 32, No. 13 ***3887–3897***
doi:10.1093/nar/gkh702

Sequence-specific artificial ribonucleases. I. *Bis*-imidazole-containing oligonucleotide conjugates prepared using precursor-based strategy

Natalia G. Beloglazova, Martin M. Fabani[1], Marina A. Zenkova*, Elena V. Bichenkova[1], Nikolai N. Polushin[2], Vladimir V. Sil'nikov, Kenneth T. Douglas[1] and Valentin V. Vlassov

Institute of Chemical Biology and Fundamental Medicine, Siberian Division of the Russian Academy of Sciences, Novosibirsk 630090, Russian Federation, [1]Wolfson Centre for Rational Design of Molecular Diagnostics, School of Pharmacy and Pharmaceutical Sciences, University of Manchester, Manchester M13 9PL, UK and [2]Fidelity Systems Inc., 7961 Cessna Avenue, Gaithersburg, MD 20879, USA

Received May 21, 2004; Revised and Accepted June 24, 2004

ABSTRACT

Antisense oligonucleotide conjugates, bearing constructs with two imidazole residues, were synthesized using a precursor-based technique employing post-synthetic histamine functionalization of oligonucleotides bearing methoxyoxalamido precursors at the 5′-termini. The conjugates were assessed in terms of their cleavage activities using both biochemical assays and conformational analysis by molecular modelling. The oligonucleotide part of the conjugates was complementary to the T-arm of yeast $tRNA^{Phe}$ (44–60 nt) and was expected to deliver imidazole groups near the fragile sequence C_{61}-ACA-G_{65} of the tRNA. The conjugates showed ribonuclease activity at neutral pH and physiological temperature resulting in complete cleavage of the target RNA, mainly at the C_{63}–A_{64} phosphodiester bond. For some constructs, cleavage was completed within 1–2 h under optimal conditions. Molecular modelling was used to determine the preferred orientation(s) of the cleaving group(s) in the complexes of the conjugates with RNA target. Cleaving constructs bearing two imidazole residues were found to be conformationally highly flexible, adopting no preferred specific conformation. No interactions other than complementary base pairing between the conjugates and the target were found to be the factors stabilizing the 'active' cleaving conformation(s).

INTRODUCTION

The design of site-specific artificial ribonucleases is one of the most challenging tasks in RNA targeting (1–17). Apart from being useful tools in molecular biology (18), such compounds may provide new possibilities for the development of novel therapeutics affecting specific messenger RNAs and viral genomic RNAs (19–21). *In vitro* experiments performed on oligonucleotides conjugated with some lanthanide complexes, showed them to display high ribonuclease activity (22–25). However, *in vivo* applications of artificial ribonucleases require these compounds to cleave RNA efficiently under physiological conditions in the absence of additional exogenous cofactors (such as metal ions, oxygen and redox reagents). Therefore, attempts have been made to develop metal-independent RNA-cleaving conjugates with cleaving constructs mimicking catalytic sites of natural ribonucleases. Potential catalytic structures composed of peptides (2–4), oligoamines (5) or imidazole-based compounds (7–9) equipped with imidazole, carboxyl and/or amino groups that normally constitute the catalytic domains of natural enzymes were conjugated to structures capable of interacting with RNA. As affinity domains intercalating dyes (7), cationic structures (8,9, 26–28) or oligonucleotides (10–17) have been used. Some of the oligonucleotide-based artificial ribonucleases were shown to cleave RNA at target sequences (10,15,17,29–32), although with poor efficiency. Therefore, further progress in this area seems to rely on both the structural study of artificial ribonucleases and the development of novel synthetic strategies to provide structural variants of cleaving constructs and ensure effective and specific RNA cleavage.

In this study, we describe oligonucleotide-based artificial ribonucleases prepared using a novel synthetic strategy, a precursor technique (33), which makes it possible to synthesize libraries of cleaving constructs with systematically varied composition and structural properties. The conjugates contain a *bis*-imidazole cleaving group covalently attached to oligonucleotide **B** via a flexible linker and an anchor group (Figure 1A). The cleaving activity of these artificial ribonucleases was assessed using yeast $tRNA^{Phe}$ to compare them with other imidazole-containing conjugates previously tested against this RNA target (16,17,31,32). The new conjugates display improved cleaving activities as compared with previous conjugates (16,17,31,32), and cleave target yeast $tRNA^{Phe}$ mainly at the target phosphodiester bond A_{63}–C_{64} adjacent to the conjugate binding site (44–60 nt). Potential structures of the complexes of conjugates with the target sequence were analysed using molecular modelling to reveal

*To whom correspondence should be addressed. Tel: +7 3832 333761; Fax: +7 3832 333677; Email: marzen@niboch.nsc.ru

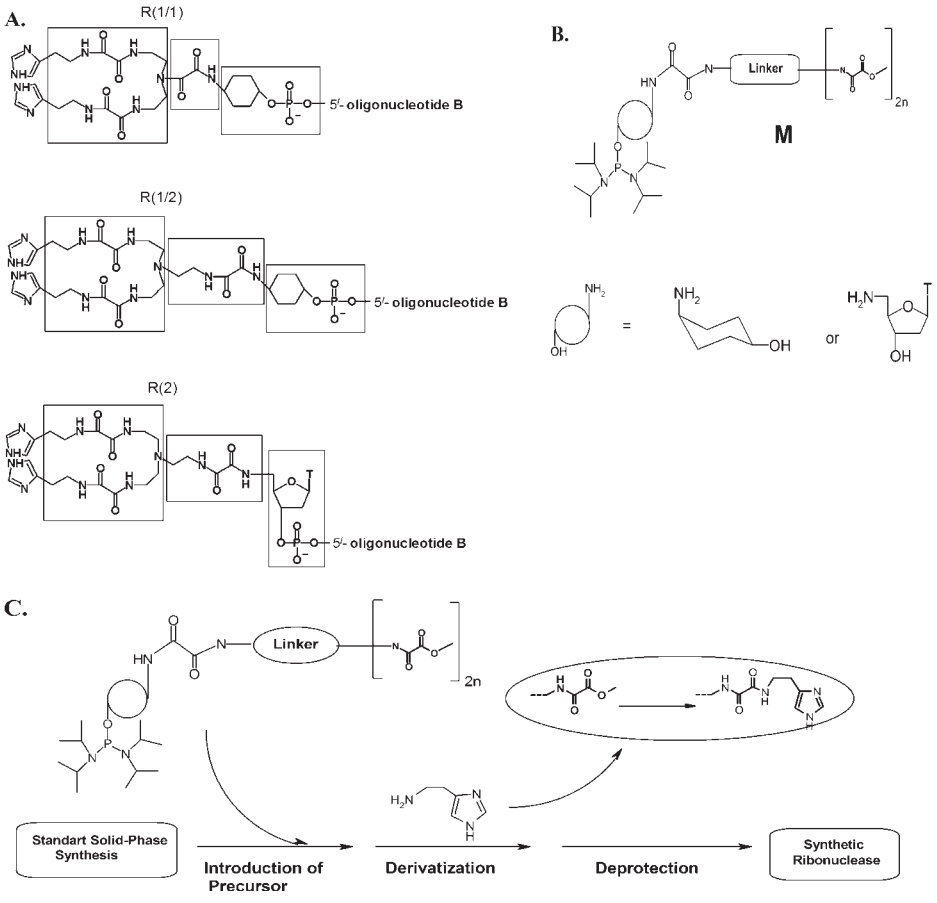

Figure 1. Imidazole-containing oligonucleotide conjugates. (**A**) Schematic representation of oligonucleotide conjugates B-R(1/1), B-R(1/2) and B-R(2). Cleaving constructs R(1/1), R(1/2) and R(2) comprise *bis*-imidazole cleaving groups, flexible linker and anchor groups (shown by solid boxes) covalently attached to the addressed oligonucleotide B via the 5′-phosphate group. (**B**) Schematic representation of the terminal modifiers (M) bearing methoxyoxaloamido (MOX) precursor groups along with a phosphoramidite moiety. (**C**) Synthesized modifiers were introduced onto the 5′-terminus of the synthetic oligodeoxyribonucleotide at the last step of an automated synthesis, resulting in the formation of the MOX-oligonucleotide precursor. The MOX precursor groups were then post-synthetically derivatized with histamine to yield oligonucleotide conjugate, bearing the imidazole-containing catalytic construct at the 5′ end.

factors affecting cleavage activity, which should be taken into account when designing new improved artificial ribonucleases.

MATERIALS AND METHODS

Yeast $tRNA^{Phe}$ was a gift from Dr G. Keith (Institut de Biologie Moleculaire et Cellulaire du CNRS, Strasbourg, France). [5′-^{32}P]pCp was from Biosan Co. (Russia). T4 RNA ligase was purchased from Fermentas (Lithuania). Methoxyoxalamido (MOX) modifiers were prepared as described previously (33). All buffers used in the experiments were prepared using MilliQ water, contained 0.1 mM EDTA and were filtered through 0.22 μm filters (Millipore).

Synthesis of oligonucleotide conjugates B-R(*n*) [Types (1/1), (1/2) and (2)]

Deoxyribooligonucleotide **B** d(GATCGAACACAGGACCT) was synthesized using standard solid-phase phosphoramidite chemistry except that dC^{Bz}-phosphoramidite was replaced by dC^{Ac}-phosphoramidite to prevent N^4-side product formation during functionalization with histamine (34). At the last stage of the automated synthesis, the core 17mer oligonucleotide was coupled with one of the modifiers M [Types (1/1), (1/2) or 2; Figure 1A and B] (0.1 M in acetonitrile) for 3 min. These oligonucleotide-MOX precursors were then functionalized with histamine (2 M in dimethylformamide) for 3 h at 20°C with constant stirring to yield (after deprotection with ammonia), oligonucleotide conjugates B-R(1/1), B-R(1/2) or B-R(2), respectively (Figure 1A and C). These oligonucleotide conjugates were purified by electrophoresis in 16% polyacrylamide/8 M urea gel under denaturing conditions. The purified conjugates were analysed using electrospray ionization and/or matrix-assisted laser desorption ionization time-of-flight mass spectrometry; for conjugates B-R(1/1), B-R(1/2) and B-R(2), experimental and calculated (in parentheses) values of molecular masses were 5523.30 (5523.73), 5566.39 (5566.80) and 5692.03 (5692.87), respectively.

Hybridization of $tRNA^{Phe}$ with oligonucleotide B

[3′-^{32}P]$tRNA^{Phe}$ was prepared according to the published protocols (35) and purified by electrophoresis in 12% polyacrylamide/8 M urea gel. The labelled tRNA was eluted from the gel, precipitated with ethanol, dried, dissolved in water and stored at −20°C. Hybridization of oligonucleotide **B** to $tRNA^{Phe}$ was analysed using gel-mobility shift assay (35).

Hybridization was performed in reaction mixtures (10 µl) containing [3′-^{32}P]tRNA at a concentration of 5×10^{-7} M, oligonucleotide **B** (ranging in concentration from 1×10^{-6} to 1×10^{-5} M), 50 mM HEPES-KOH, pH 7.5, 200 mM KCl and 0.1 mM EDTA at 37°C for 4 h. After incubation, 8 µl of loading buffer (50% glycerol, 0.025% bromophenol blue, 0.025% xylene cyanol) was added to the probe and the probes were analysed by electrophoresis in native 10% polyacrylamide gel at 4°C using 100 mM Tris–borate running buffer (pH 8.3) at 350 V for 6 h. To quantify the data, the gels were dried, radioactive bands were cut out and their radioactivity determined by Cherenkov counting.

Probing the tRNA^{Phe} structure in the complex with oligonucleotide B

Probing was carried out using RNase H (36) and 2 M imidazole buffer, pH 7.0. Hybridization reactions were prepared and incubated as described above. RNase H (1–1.5 U; Promega) was added to the mixtures in buffer, supplemented with 2 mM dithioerythritol (DTE) and incubated for 2 h at 20°C. Probing with 2 M imidazole buffer was performed as described previously (37) at 37°C for 12 h. The reactions were quenched by precipitation of tRNA with a solution of 2% lithium perchlorate in acetone (150 µl). RNA was collected by centrifugation and dissolved in loading buffer (6 M urea, 0.025% bromophenol blue and 0.025% xylene cyanol), and the products were analysed by electrophoresis in 12% polyacrylamide/8 M urea gel. Partial RNase T1 digests were run in parallel with RNase H cleavage products to identify the cleavage sites (38).

Cleavage of tRNA^{Phe} with oligonucleotide conjugate B-R(*n*)

The reaction mixture (10 µl) contains 50 mM imidazole buffer, pH 7.0, 200 mM KCl, 1 mM EDTA, 100 µg/ml total tRNA from *Escherichia coli* as carrier, 5×10^{-7} M [3′-^{32}P]tRNA^{Phe} and oligonucleotide conjugates B-R(1/1), B-R(1/2) or B-R(2) at concentrations ranging from 5×10^{-7} to 5×10^{-4} M (as indicated in the legends to the figures). The reactions were carried out at 37°C for various incubation times and quenched by precipitation of tRNA and tRNA fragments with 2% lithium perchlorate solution in acetone (150 µl). RNA was collected by centrifugation, dissolved in loading buffer (6 M urea, 0.025% bromophenol blue and 0.025% xylene cyanol) and analysed by electrophoresis in 12% polyacrylamide/8 M urea gel. An imidazole-ladder and a G-ladder produced by partial RNA cleavage with 2 M imidazole buffer, pH 7.0 (37) and RNase T1 (38) were run in parallel. Quantitative data were obtained as described above. The total extent of tRNA cleavage was determined as the ratio of radioactivity measured in the tRNA fragments to the total radioactivity applied to the gel.

Kinetics of RNA cleavage

The reaction mixtures were prepared and analysed similar to the procedure described above. Briefly, reaction mixtures (100 µl) containing 5×10^{-7} M [3′-^{32}P]tRNA^{Phe}, 50 mM imidazole buffer, pH 7.0, 200 mM KCl, 1 mM EDTA, 100 µg/ml total tRNA from *E.coli* as carrier and oligonucleotide conjugates B-R(1/1), B-R(1/2) or B-R(2) at concentrations ranging from 1×10^{-6} to 5×10^{-5} M were incubated at 37°C. At defined time periods, aliquots (10 µl) were withdrawn from the reaction mixtures, quenched by precipitation with 2% lithium perchlorate solution in acetone (150 µl) and analysed as described above. The kinetics of RNA cleavage by the conjugates was analysed quantitatively in terms of consecutive reactions (Scheme 1).

$$\text{tRNA} + \text{B-R(1/1)} \underset{k_{-1}}{\overset{k_1}{\rightleftharpoons}} \text{tRNA}\bullet\,\text{B-R(1/1)} \xrightarrow{k_2} \text{P1} + \text{P2}\bullet\,\text{B-R(1/1)}$$

Scheme 1.

In Scheme 1, k_1 and k_{-1} are the rate constants for hybridization and dissociation of the duplex, respectively, and k_2 is the effective rate constant for cleavage yielding P1 and P2 as 3′ and 5′ tRNA fragments, respectively. The concentration of the labelled [3′-^{32}P]tRNA^{Phe} was held constant (0.5 µM), and that of the conjugates varies from 1 to 50 µM. As the conjugate concentration was much higher than that of tRNA^{Phe}, the experimental data were analysed using pseudo first-order kinetics with the approximation that the concentration of B-R(*n*) was effectively constant. Under the experimental conditions, the heteroduplex formed by the tRNA and the oligonucleotide part of the conjugate is highly stable, indicating very slow hybrid dissociation (i.e. $k_1 \gg k_{-1}$). Under these conditions, the equation describing the time dependence on the extent of cleavage (α) is given by Equation 1:

$$\alpha = 100\% \cdot \left(1 - \frac{k_2}{k_2 - k_1} e^{-k_1 t} + \frac{k_1}{k_2 - k_1} e^{-k_2 t}\right), \qquad \mathbf{1}$$

where t is time, and k_1, k_{-1} and k_2 are the rate constants (Scheme 1). Global fitting of the data obtained from several experiments and several conjugate concentrations was used to determine k_1 and k_2 using Origin 6.0 software.

Molecular modelling

Molecular modelling was performed on a Silicon Graphics O2 workstation using SYBYL 6.6 (TRIPOS Inc.). All Molecular Mechanics (MM) and Molecular Dynamics (MD) calculations were carried out *in vacuo* using Kollman-All force field parameters. During MM/MD runs, a distance-dependent dielectric constant of 4 was used with an integration time step of 1 fs.

Three model systems representing complexes of tRNA^{Phe} with the conjugates as heteroduplexes, H-R(1/1), H-R(1/2) and H-R(2), were assessed by molecular modelling. An A-like DNA:RNA hybrid was built using BIOPOLYMER/SYBYL 6.6. The non-standard fragments, R(1/1), R(1/2) and R(2), were built using SKETCH/SYBYL 6.6. The parameterization and the calculation of charge distributions for these constructs were performed using MOPAC program (39) after geometric optimization. The cleaving fragment was attached to the DNA:RNA hybrid via the terminal 5′-phosphate group of the G_1 nucleotide residue followed by an energy minimization procedure to remove any unfavourable Van der Waals contacts.

The nomenclature used in the description of the modelled duplexes was as follows. R(*n*) indicates the linker–cleaver assembly; H preceding this refers to a heteroduplex. In various steps of the calculations the letter H is replaced variously: S, starting conformation; F, final conformation; and O, optimal conformation.

For each molecule [H-R(1/1), H-R(1/2) and H-R(2)] various starting structures were created, differing in the location of the cleaving group, ranging from 'in' to 'out' extreme positions relative to the DNA:RNA hybrid. H-R(1/1) gave rise to S1-R(1/1)–S6-R(1/1) starting structures; H-R(1/2) gave S1-R(1/2)–S6-R(1/2) and H-R(2) gave S1-R(2)–S6-R(2) starting structures, respectively. Prior to MD calculations, the starting structures of each molecule were subjected to energy minimization to a gradient convergence of 0.05 kcal/mol, considering the DNA:RNA hybrid as a solid body. In the next stage, each starting structure was individually subjected to a 12 ps MD run using a simulated-annealing protocol as follows. The system was heated to 600 K for 2 ps followed by gradual cooling to 100 K for 10 ps. A final minimization to convergence was performed resulting in the respective final conformations for each type of molecule [H-R(1/1), F1-R(1/1)–F6-R(1/1); H-R(1/2), F1-R(1/2)–F6-R(1/2); and H-R(2), F1-R(2)–F6-R(2)].

'Active conformations' [O-R$(1/1)_{63–64}$, O-R$(1/2)_{63–64}$ and O-R$(2)_{63–64}$] were obtained using a similar simulated-annealing protocol. The cleaving groups within these molecules were deliberately located in the most favourable position for successful cleavage at the C_{63}–A_{64} site using distance constraints. The structural organization of the 'reactive complex' was based both on the conventional mechanism of RNA cleavage by RNase A (40) and on the available coordinate sets for the RNase A complex with a substrate or a product analogue (41–43). According to these data, the distance between the imidazole unit of the first histidine moiety and the anionic phosphate oxygen of the nucleic acid is in the range 2.6–3.5 Å, whereas the distance between the imidazole unit of the second histidine unit and the 2′-OH group of the same nucleotide lies in the range 3.1–3.7 Å. Therefore, the constraint between N1 of one of the imidazole residues and 2′-OH group of C_{63} was set to an average value (3.0 Å), and the distance between N1 of the other imidazole residue and the non-bridged oxygen of the phosphate group, connecting C_{63} and A_{64}, was also set to 3.0 Å (41,44) with the force constants of 50 kcal/mol. A final minimization was performed without constraints, using the above protocol.

The 'active conformations' for the C_{61}–A_{62} potential cleavage site [O-R$(1/1)_{61–62}$, O-R$(1/2)_{61–62}$ and O-R$(2)_{61–62}$] were obtained similar to those for the C_{63}–A_{64} cleavage site by deliberately positioning the imidazole cleaving groups near the C_{61}–A_{62} site. However, in this case higher force constants (300 kcal/mol) were used to satisfy the requirements for optimal orientation of cleaving groups (i.e. 3.0 Å from the C_{61}–A_{62} site).

RESULTS

Application of MOX precursor strategy to the synthesis of artificial ribonucleases

The efficiency of the MOX precursor (MOX modifiers) approach has been demonstrated previously in the synthesis of 2′-modified oligonucleotides (45). Recently, this strategy was applied to the oligonucleotide 5′-functionalization (33). 5′-MOX modifiers can be prepared in two steps from virtually any molecule containing two functional groups, an aliphatic primary amino group and a hydroxyl group (Figure 1, Supplementary Material). First, the amino group is transferred to the MOX group on treatment with excess dimethyl oxalate. Treatment of the reaction products with tris(2-aminoethyl) amine leads to a molecule with two aliphatic amino groups connected to the starting compound by a flexible linker. These steps can be repeated several times to yield branched molecules bearing a number of groups available for further functionalization (Figure 1, Supplementary Material). Then the hydroxyl group is phosphitylated in the standard way. Both steps are robust and proceed with a high yield. To prepare the 5′-MOX modifiers of Type 1 and Type 2, *trans*-4-aminocyclohexanol and 5′amino-5′deoxythymidine were used, respectively (Figure 1B).

The RNA-cleaving oligonucleotide conjugates were prepared by a two-step procedure (33). First, the precursor 17mer d(GATCGAACACAGGACCT) (**B**) was synthesized and elaborated with 5′-MOX modifiers of different types [Types (1/1), (1/2) or (2)] at the last step of synthesis. These oligonucleotide MOX precursors were then functionalized with histamine (see Materials and Methods) and further deprotected with ammonia to yield oligonucleotide conjugates bearing two histamine residues at the 5′ end (Figure 1C). Figure 1A provides structures of three oligonucleotide conjugates studied in this work, hereafter referred to as B-R(1/1), B-R(1/2) and B-R(2). Conjugates B-R(1/1) and B-R(1/2) slightly differ from each other in linker length, and conjugates B-R(1/2) and B-R(2) in the nature of anchor group [a cyclohexyl moiety in B-R(1/1) and B-R(1/2), or a thymidine residue in B-R(2)].

Hybridization assay

$tRNA^{Phe}$ was chosen deliberately as the target to assess cleavage activity of artificial ribonucleases because other types of oligonucleotide-based artificial ribonucleases containing two imidazole residues had been tested using this target (10,12,15,16,31). Moreover, hybridization of antisense oligonucleotides with yeast $tRNA^{Phe}$ has been investigated in detail (36,46–49) providing useful background for comparison. Finally, we take advantage of using a well-studied natural RNA (50,51), short enough to detect cleavage patterns directly (using end-labelled RNA species), and with a well-known structure with elements (loops, stems, junctions, etc.) common in natural RNAs.

Figure 2A represents the cloverleaf structure of yeast $tRNA^{Phe}$ showing the target site for the designed artificial ribonucleases B-R(*n*) with the addressing 17mer oligonucleotide **B** complementary to the $tRNA^{Phe}$ sequence 44–60. Hybridization of **B** with the 44–60 sequence results in the delivery of catalytic groups to the two adjacent CA bonds in the sequence $C_{61}ACAG_{65}$. 5′-Py-A-3′ sequences in RNA are highly susceptible to cleavage by RNase A and imidazole-containing chemical ribonucleases (26,31,52).

In the absence of magnesium ions oligonucleotide **B** binds efficiently to its complementary sequence in $tRNA^{Phe}$, with 90% complex formation at an oligonucleotide concentration of 5×10^{-5} M (49). Specificity of oligonucleotide **B** binding to $tRNA^{Phe}$ was investigated by probing with RNase H and by 2 M imidazole buffer. Samples of [3′-^{32}P]$tRNA^{Phe}$ were incubated with oligonucleotide **B** and subjected to partial cleavage with RNase H and 2 M imidazole buffer, pH 7.0

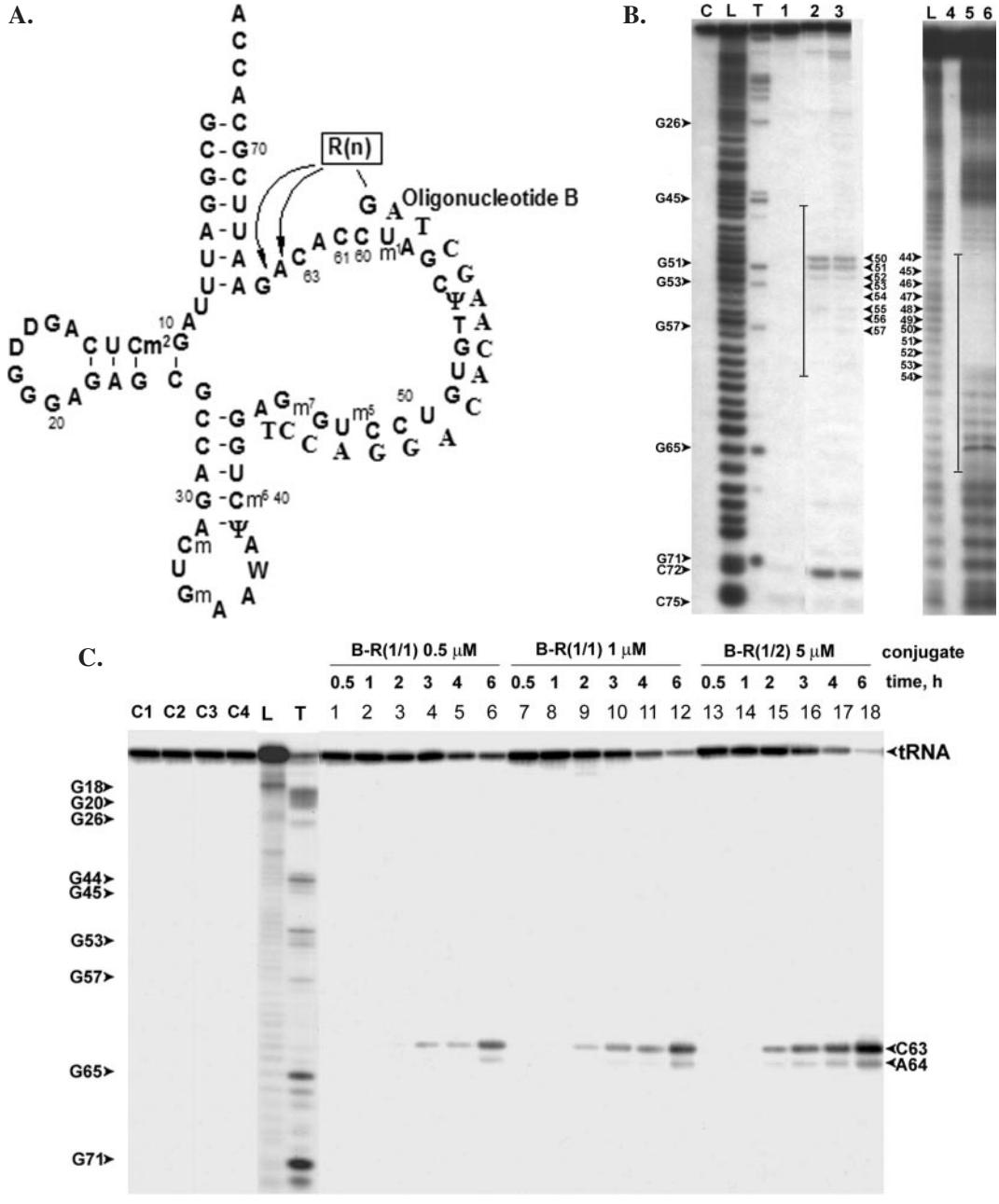

Figure 2. Cleavage of $tRNA^{Phe}$ by oligonucleotide conjugates B-R(1/1) and B-R(1/2). (**A**) Cloverleaf structure of yeast $tRNA^{Phe}$ and the target sequence for oligonucleotide **B**-based artificial ribonucleases B-R(*n*) [R(*n*) is the RNA-cleaving construct shown in Figure 1). Arrows indicate the sites of tRNA cleavage by the oligonucleotide conjugates. (**B**) RNase H and imidazole-buffer probing of the $tRNA^{Phe}$ structure in the complex with oligonucleotide **B**. Autoradiograph of 12% polyacrylamide/8 M urea gel after separation of [3′-^{32}P]$tRNA^{Phe}$ and cleavage products. Lanes: C, intact tRNA; L and T, tRNA partial cleavage by 2 M imidazole buffer, pH 7.0 and by RNase T1 under denaturing conditions, respectively; 1 and 4, tRNA cleaved by RNase H (0.25 U) or 2 M imidazole buffer in the absence of oligonucleotide **B** at 20°C for 2 and 12 h, respectively; 2 and 3, tRNA cleaved by RNase H (0.25 and 0.5 U, respectively) in the complex with oligonucleotide **B** (5×10^{-6} M) at 20°C for 2 h; 5 and 6, tRNA hydrolyzed by 2 M imidazole buffer in the complex with oligonucleotide **B** (5×10^{-6} M) at 37°C for 12 and 18 h, respectively. Solid lines indicate oligonucleotide **B** complementary region. (**C**) Autoradiograph of 12% polyacrylamide/8 M urea gel. Cleavage reactions were performed as described in Materials and Methods. Lanes: C1, $tRNA^{Phe}$ incubated in the reaction buffer at 37°C for 5 h; C2, $tRNA^{Phe}$ incubated in the reaction buffer in the presence of 1×10^{-6} M oligonucleotide **B** at 37°C for 5 h; C3, $tRNA^{Phe}$ incubated in the reaction buffer in the presence of 1×10^{-6} M cleaving construct R(2) at 37°C for 5 h; C4, $tRNA^{Phe}$ incubated in the reaction buffer in the presence of an equimolar mixture of oligonucleotide **B** and cleaving construct R(2) at 37°C for 5 h; L, ladder produced by 2 M imidazole buffer; T, partial digest with RNase T1; lanes 1–6, incubation of $tRNA^{Phe}$ with 5×10^{-7} M conjugate B-R(1/1); lanes 7–12, incubation of $tRNA^{Phe}$ with 1×10^{-6} M conjugate B-R(1/1); lanes 13–18, incubation of $tRNA^{Phe}$ with 5×10^{-6} M conjugate B-R2(1/2) each for 0.5, 1, 2, 3, 4 and 6 h, respectively.

(Figure 2B). This probing provides evidence that oligonucleotide **B** forms a complex with the target sequence (Figure 2B, lanes 2, 3 and 5, 6). The main cleavage sites on treatment with RNase H were at positions 50, 51 and 52, whereas positions 53–57 within the target site were cleaved less efficiently. Under these conditions, several cuts were observed at sites distant from the complementary sequence (U_8–A_9, C_{13}–A_{14}, C_{72}–A_{73} and C_{75}–A_{76}), and resulted from non-specific tRNA

cleavage at the single-stranded CA and UA motifs, known to be sensitive towards cleavage by various agents. RNase H cleavage sites overlap with the tRNA region protected from cleavage by 2 M imidazole buffer by hybridization with oligonucleotide **B** (positions 44–54; Figure 2B, lanes 4 and 5). Figure 2B shows that sequence 55–60 of $tRNA^{Phe}$ was less protected from cleavage than residues 40–54, also involved in the RNA:DNA hybrid formation. This is consistent with a lower stability of the heterocomplex formed by the 5′-part of oligonucleotide **B** with the tRNA due to the presence of the m^1A_{58} residue in this tRNA region, which is known to be incapable of base pairing. Probing the $tRNA^{Phe}$ structure with RNase ONE™ ribonuclease in the course of its hybridization with an 18mer oligonucleotide complementary to the 44–61 tRNA sequence indicated that the heteroduplex formation results in unfolding of the TΨC hairpin of tRNA and does not disturb the secondary structural elements of the rest of the tRNA molecule (49).

Cleavage of yeast $tRNA^{Phe}$ by the conjugates B-R(1/1), B-R(1/2) and B-R(2)

[3′-^{32}P]$tRNA^{Phe}$ (5×10^{-7} M) was incubated with conjugates B-R(1/1), B-R(1/2) and B-R(2) at conjugate concentrations ranging from 5×10^{-7} to 5×10^{-4} M in imidazole buffer at 37°C (see Materials and Methods). These conditions correspond to single-turnover reaction conditions (53,54) and thus provide reliable kinetic data for comparisons of cleaving activity of the conjugates as the hybridization proceeds similar over this concentration range. Figure 2C displays a typical $tRNA^{Phe}$ cleavage pattern obtained after incubation with conjugates B-R(1/1) and B-R(2). Conjugates B-R(1/1) and B-R(2) exhibited similar cleavage specificities with the major cut at the C_{63}–A_{64} bond and to a lesser extent at A_{64}–G_{65} in the target sequence in the T-arm of the $tRNA^{Phe}$ [primary data for conjugate B-R(1/2) not shown]. The source of the difference in cleavage efficiency at sequences C_{63}–A_{64} and A_{64}–G_{65} could be due to different accessibilities and sensitivities of these phosphodiester bonds towards the catalysts. Phosphodiester bond A_{64}–G_{65} seems to be more resistant to cleavage, as scission of this bond requires a longer incubation time. $tRNA^{Phe}$ cleavage at the A_{64}–G_{65} bond (together with strong cleavage at C_{63}–A_{64}) in the presence of imidazole-containing chemical ribonucleases has been observed previously (26,27). No cleavage at phosphodiester bond A_{61}–C_{62}, even after long incubation, was observed. This can be explained by increased rigidity of the phosphodiester bond adjacent to the heteroduplex, which interferes with the transesterification step. An additional reason for A_{61}–C_{62} cleavage resistance, was obtained by molecular modelling (see below), which revealed poor accessibility of this site due to steric hindrance. Less efficient cleavage of phosphodiester bonds adjacent to conjugate complementary sequences have been reported previously (16).

The cleavage products migrated similar to oligonucleotides generated by RNase T1 or by 2 M imidazole buffer (Figure 2C, lanes L and T, respectively) indicating formation of a cyclic phosphodiester at the 3′-cleavage site, and a hydroxyl group in the 5′-cleavage products. No measurable spontaneous degradation of the tRNA was observed under experimental conditions in the absence of the conjugate (Figure 2C, lane C1), in the presence of parent oligonucleotide **B** alone (Figure 2C, lane C2), in the presence of the cleaving group Type 2 alone (Figure 2C, lane C3), or in an equimolar mixture of oligonucleotide **B** and the cleaving group Type 2 (Figure 2C, lane C4), after incubation for 5 h.

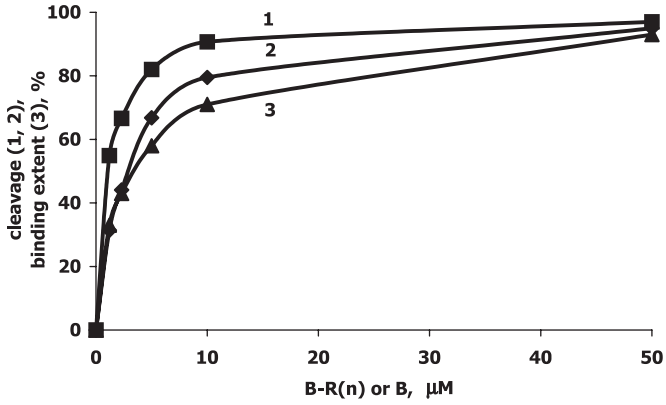

Figure 3. Influence of concentration of conjugates B-R(1/1) (curve 1) and B-R(1/2) (curve 2) on the efficiency of $tRNA^{Phe}$ cleavage: [3′-^{32}P]$tRNA^{Phe}$ (5×10^{-7} M) was incubated at 37°C for 4 h in 50 mM imidazole buffer, pH 7.0, containing 200 mM KCl, 0.1 mM EDTA and 100 μg/ml RNA carrier in the presence of conjugate. Curve 3 represents the extent of binding of parent oligonucleotide **B** to $tRNA^{Phe}$ under the same conditions (see Figure 2B).

Comparison of the dependences of tRNA cleavage versus conjugate concentration for conjugates B-R(1/1), B-R (1/2) and the extent of binding of the parent oligonucleotides **B** (Figure 3) indicate that conjugation of the RNA-cleaving group to the 5′ end of the oligonucleotide does not affect the hybridization efficiency: nearly plateau values of cleavage were achieved at a conjugate concentration of 10 μM, which corresponds to 70% of tRNA bound to conjugate. The differences between extent of binding (curve 3) and extent of tRNA cleavage (curves 1 and 2) at each given concentration can be attributed to the fact that binding represents an equilibrium reaction, whereas cleavage is an irreversible process, thus indicating that dissociation of the conjugate from the duplex with RNA cleavage products takes place.

The kinetics of RNA cleavage by the conjugates is sigmoidal with an initial lag period, whose duration depends on the nature of the conjugate (Figure 4A). At low conjugate concentrations (i.e. at concentrations equal to or close to that of the target RNA), the sigmoidicity of the curve is more pronounced, reflecting a complex mechanism for the reaction involving several steps. The first step is hybridization of the conjugate to the RNA as a bimolecular reaction, depending on the concentration of both interacting molecules (Scheme 1). At low concentrations of the conjugate, hybridization occurs rather slowly (36,49), and it takes a measurable time for the complementary complex to be formed, which results in a noticeable lag period. Formation of the duplex provides the possibility of cleavage. At higher conjugate concentrations, hybridization occurs more rapidly, and both processes (hybridization and cleavage) proceed with similar rates, resulting in a decreased initial lag period. At high concentrations of the conjugate cleavage rather than hybridization becomes the rate-limiting step.

The kinetics of RNA cleavage with conjugate B-R(1/1) was analysed quantitatively in terms of consecutive first-order

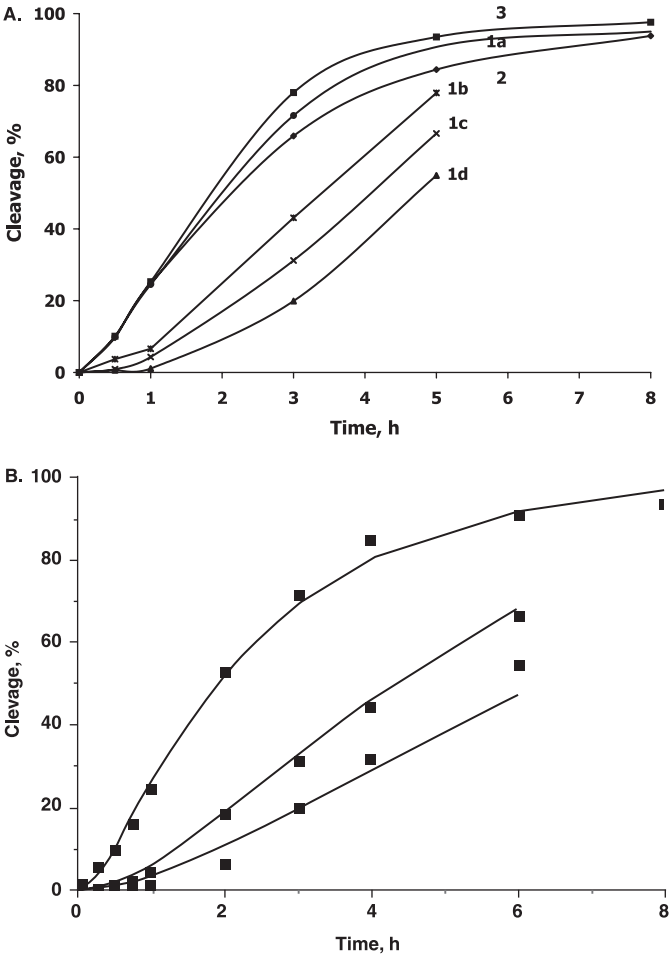

Figure 4. The kinetics of $tRNA^{Phe}$ cleavage with oligonucleotide conjugates B-R(*n*). (**A**) The kinetics of $tRNA^{Phe}$ cleavage by conjugate B-R(1/1) at 10.0, 5.0, 1.0 and 0.5 μM (curves 1a, 1b, 1c and 1d, respectively), and conjugates B-R(1/2) and B-R(2) at 10.0 μM (curves 2 and 3, respectively). Cleavage reactions were performed at 5×10^{-7} M [3′-^{32}P]$tRNA^{Phe}$ in 50 mM imidazole buffer, pH 7.0, containing 200 mM KCl, 1 mM EDTA, 100 μg/ml RNA carrier at 37°C. (**B**) The solid lines represent the fitting of experimental data [curves 1a, 1c and 1d in (A)] for the $tRNA^{Phe}$ cleavage with conjugate B-R(1/1) to a three-state model of consecutive first-order reactions (Scheme 1).

reactions (see Materials and Methods). Global fitting (shown in Figure 4B) of the data from several experiments according to Equation 1 gave $k_1 = 99.4 \pm 5.2$ M^{-1} s^{-1} and $k_2 = 1.2 \pm 0.05$ s^{-1}. The value of hybridization rate constant derived from the kinetics of the tRNA cleavage is consistent with the hybridization rate constant of oligonucleotide **B** measured using gel-mobility shift assay (49). The calculated rate constant k_1 ($\sim 10^2$ M^{-1} s^{-1}) is rather low compared with known rate constants for duplex formation between two linear strands [$k_1 = 10^5$–10^6 M^{-1} s^{-1} at 23°C (55)] or hybridization of antisense RNA with its sense counterpart [$k_1 = 10^3$–10^4 M^{-1} s^{-1}; (56–58)]. This slow hybridization indicates the stability of the tRNA structure and reflects the cost of local unfolding of the tRNA structure. The rate constant (k_2) characterizing the cleavage reaction *per se* is also not high.

For comparative purposes, we have collected relative rates of cleavage as the times required for 50% cleavage to occur ($\tau_{1/2}$). The conjugates cleave RNA at similar rates characterized by reaction half-life times of the order of 2 h [1.5, 2.1 and 2.2 h for conjugates B-R(1/1), B-R(1/2) and B-R(2), respectively]. The conjugate B-R(1/1) consistently exhibited the highest rate for site-directed RNA cleavage.

Molecular modelling of tRNA–conjugate complexes

The main priority of the molecular modelling was to identify possible location(s) of cleaving group(s) relative to the main scissile $^{5'}C_{63}$–A_{64} site and correlate structural properties of hybridized conjugates with their hydrolytic activity.

As a first approximation, the complex between TΨC region of tRNA and oligonucleotide **B** was modelled by using a shortened double-stranded DNA:RNA duplex, comprising the 44–66 nt fragment of the TΨC hairpin of $tRNA^{Phe}$. It was shown in previous experiments (36,46–49) that complementary oligonucleotides can effectively invade this hairpin structure in the absence of magnesium ions. Successful hybridization of complementary oligonucleotides with the 44–60 tRNA sequence disrupts its three-dimensional structure (49), since nucleotides in the TΨC loop are involved in the maintenance of tRNA tertiary structure (59). The study of the effects of $MgCl_2$ and temperature on the structural and dynamic properties of yeast $tRNA^{Phe}$ confirmed significant destabilization of the acceptor stem, the D stem and the tertiary structure in the absence of Mg^{2+} ions at high temperature (40°C) (59–61). These evidences, in tandem with this study (Figure 2B), strongly suggest that under these experimental conditions (presence of oligonucleotide **B** or conjugate, absence of Mg^{2+} ions and an elevated temperature of 37°C) the tertiary structure of the tRNA molecule is disrupted. An earlier study (49) has also shown that hybridization with a complementary oligonucleotide results in TΨC hairpin unfolding (Figure 1C), implying that this region is not involved in the formation of the tertiary structure. Therefore, this shortened double-stranded DNA:RNA model duplex appears to be a reasonable approximation for molecular modelling purposes. For this purpose, we assumed an A-like conformation based on physicochemical (62), X-ray (63) and NMR/molecular modelling evidence (64). This DNA:RNA hybrid, comprising a target RNA sequence ($^{5'}A_{44}$–U_{69} fragment of $tRNA^{Phe}$) and an oligonucleotide conjugate is shown in Figure 2A (see also Supplementary Material, Figure 2). Based on this hybrid duplex, three model molecules were created [H-R(1/1), H-R(1/2) and H-R(2)]. In the absence of detailed structural data for the DNA:RNA hybrid, it was reasonable to treat the hybrid as a solid structure while allowing cleaving constructs to possess full conformational flexibility during the calculations. For each molecule [H-R(1/1), H-R(1/2) and H-R(2)] several starting structures were created, differing in the spatial orientations of the cleaving construct(s), ranging from 'in' to 'out' conformational extremes. All starting structures were subjected to independent simulated-annealing experiments giving rise to the respective final structures. Structural parameters and energy values of each final structure were analysed and compared with those of 'active' conformations [O-R(1/1), O-R(1/2) and O-R(2)], which had their cleaving constructs deliberately pre-organized by mimicking structural parameters of RNase A catalytic centres (41–43, 65–67) (see Materials and Methods). Table 1 contains the data for these *bis*-imidazole-containing molecules.

Table 1. Energies and distances between imidazole residues of the conjugates and phosphodiester bonds C_{60}–A_{61} and C_{63}–A_{64} of $tRNA^{Phe}$ for *bis*-imidazole-containing RNA-cleaving compounds

Molecule	Conformer	Energy (kcal/mol)	ΔE (kcal/mol)	Distance to C_{61}–A_{62} (Å)		Distance to C_{63}–A_{64} (Å)	
				Im1-OH	Im2-OP	Im1-OH	Im2-OP
H-R(1/1)	F1-R(1/1)	161.1	−13.8	7.3	15.5	10.9	11.4
	F2-R(1/1)	163.9	−11.0	7.6	13.6	15.2	12.7
	F3-R(1/1)	186.8	11.9	15.8	29.0	15.5	27.6
	F4-R(1/1)	172.0	−2.9	17.6	17.7	17.7	14.5
	F5-R(1/1)	177.3	2.4	12.3	23.8	11.9	23.1
	F6-R(1/1)	176.8	1.9	13.4	19.3	14.7	15.8
	O-R(1/1)$_{63–64}$	174.9	—	13.5	13.7	3.1	4.0
	O-R(1/1)$_{61–62}$	180.9	6.0	3.2	4.5	15.5	12.9
H-R(1/2)	F1-R(1/2)	61.5	10.3	17.6	22.7	22.7	23.7
	F2-R(1/2)	56.5	5.3	12.6	24.2	14.5	15.8
	F3-R(1/2)	49.0	−2.2	8.3	22.9	13.3	15.6
	F4-R(1/2)	49.8	−1.4	16.5	16.9	5.4	8.6
	F5-R(1/2)	58.4	7.2	10.1	21.5	8.2	17.8
	F6-R(1/2)	61.3	10.1	22.4	18.7	8.6	24.0
	O-R(1/2)$_{63–64}$	51.2	—	11.7	13.5	3.1	3.1
	O-R(1/2)$_{61–62}$	55.8	4.6	3.6	3.4	11.4	14.4
H-R(2)	F1-R(2)	5.9	17.2	20.2	24.1	18.7	19.1
	F2-R(2)	−4.3	7.0	24.4	28.2	23.3	23.5
	F3-R(2)	4.4	15.7	21.4	19.2	22.8	16.1
	F4-R(2)	−15.3	−4.0	8.7	18.5	6.4	9.9
	F5-R(2)	5.7	17.0	9.8	20.7	5.8	15.1
	F6-R(2)	1.8	13.1	16.6	21.3	14.1	15.3
	O-R(2)$_{63–64}$	−11.3	—	11.9	14.2	3.2	3.7
	O-R(2)$_{61–62}$	7.4	18.7	3.0	3.2	15.4	13.7

ΔE is the difference in energy of the conformer and the optimized [O-R(*n*)] conformer.

We analysed the possibility of location of the imidazole residues in close proximity to the C_{61}–A_{62} potential cleavage site. The molecular modelling calculations revealed that under normal simulation conditions (distance restraints of 3.0 Å, force constant of 50 kcal/mol) it was impossible to satisfy the requirements of obtaining a stable conformation with the imidazole rings located only 3 Å away from the C_{61}–A_{62} site. The only way to obtain this 'optimal conformation' was to increase force constants to 300 kcal/mol. The energies of such conformations O-R(n)$_{61–62}$ were always greater than energies of the respective conformations O-R(n)$_{63–64}$ (see Table 1). This implies that the conformations O-R(n)$_{61–62}$ (where the cleaving constructs are located near the C_{61}–A_{62} site) are less likely to occur compared with the respective O-R(n)$_{63–64}$ conformations, again suggesting a lower probability for cleaving groups to reach $^{5'}C_{61}$–A_{62} site.

Molecular modelling showed that the *bis*-imidazole cleaving constructs in molecules H-R(1/1), H-R(1/2) and H-R(2) have high conformational flexibility. No preferred specific conformation was found for these groups regardless of their initial position, which ranged from 'in' to 'out' extremes in their respective starting structures. During simulated-annealing experiments, the distances between the imidazole rings and the target RNA atoms (C2′-OH-group of C_{63} and an internucleotide phosphate group between C_{63} and A_{64}) changed randomly, possibly implying an absence of interactions between the cleaving groups and the hybrid strong enough to stabilize an 'active' conformation.

All final structures of H-R(1/1) molecule showed relatively large distances between the imidazole rings and the RNA target site, ranging from 10 to 18 Å [see Figure 5, showing F5-R(1/1) final structure as an example]. This suggests a low probability for these groups to be located close to the cleavage site (Table 1).

In the case of H-R(1/2), some final conformations demonstrated closer location of cleaving groups relative to the target site compared with H-R(1/1) (e.g. see F4-R(1/2); Table 1). This could be explained by the slightly longer linker group for H-R(1/2) compared with H-R(1/1), which can provide a higher probability of reaching the cleavage site. In general, 'short-distance' conformations seem to be more energetically favourable than 'out' conformations. These data may suggest a greater expected cleavage activity for H-R(1/2). However, biochemical assay data on H-R(1/2) showed cleavage activity ($\tau_{1/2} = 2.2$ h) similar to that obtained for H-R(1/1). Perhaps the increased conformational freedom of the cleaving groups in the H-R(1/2) molecule decreases the probability of achieving a favourable conformation.

For hybrid H-R(2), the optimal conformation O-R(2) corresponds to a low-energy state (Table 1). Only one final conformation, F4-R(2), was found, and had an even lower energy than O-R(2). It was characterized by a reasonably close location of imidazole groups to the cleavage site. However, simulated-annealing runs also gave several final conformations [F1-R(2), F2-R(2), F3-R(2) and F5-R(2)] with very distant locations of the cleaving groups from the C_{63}–A_{64} site (Table 1).

Based on the modelling data, it can be concluded that the cleaving activity of *bis*-imidazole-containing molecules H-R(1/1), H-R(1/2) and H-R(2) can be characterized as a random event, which, apart from the hybridization to give duplex, does not involve any particular pre-scaffold conformation and/or interactions of the cleaving groups with the target site.

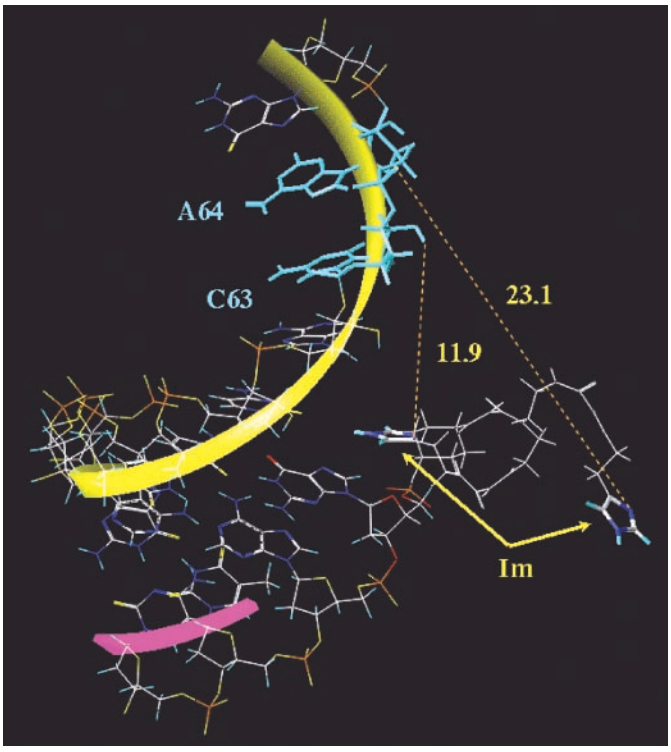

Figure 5. A fragment of F5-R(1/1) final structure representing one of the probable conformations of the B-R(1/1) molecule, and showing the possible orientation of the cleaving groups. The C_{63}–A_{64} cleavage site is shown in cyan; distances (Å) between the imidazole groups and target atoms of cleavage site are indicated.

DISCUSSION

Various RNA-cleaving catalysts have been tethered to the 5′-termini of oligonucleotides (12,16,31,32,68,69). The synthetic methods developed, except for a few examples (11), allow incorporation of only one functional moiety per phosphoramidite unit. Generally, 5′-tethering can be implemented in two ways. First, by the direct introduction of a suitably protected and activated construct onto the 5′-terminus at the end of standard solid-phase synthesis. In this case, synthesis of highly modified oligonucleotides becomes somewhat problematic because a number of incorporations should substantially decrease the overall yield of the oligonucleotides conjugate. Alternatively, a precursor molecule may be first formed by reacting with the 5′-OH group of an assembled oligonucleotide with a heterobifunctional reagent (first modifier) bearing both the phosphoramidite moiety and an reactive group. The reactive group of the precursor oligonucleotide is then post-synthetically derivatized with an appropriate functional additive (second modifier). This precursor strategy has the obvious advantage that the same parent compound can be used to fabricate a vast number of differently tethered products. In this study, the precursor-based methodology was successfully applied to the synthesis of artificial ribonucleases. The conjugates display pronounced ribonuclease activity and are capable of cleaving yeast $tRNA^{Phe}$ at two phosphodiester bonds within the target sequence. The conjugates exhibited ribonuclease activity higher than that of molecules reported previously [oligonucleotide derivatives bearing ethylenediamine or propylenediamine at the 5′-terminus (10,68,69), conjugates of oligonucleotides with structures containing imidazole residues (15,16,31,68), imidazole and amino groups (17)], and take advantage of simple and reliable synthetic procedures and the possibility to varying the structure of the catalytic part of the molecule easily.

High activity of the conjugates in the site-specific cleavage of $tRNA^{Phe}$ was achieved, probably by efficient hybridization of the parent oligonucleotide (37,46–49), and by selection of an RNA sequence that is particularly sensitive towards the catalyst. The catalytic part of the conjugates has little or no effect on hybridization. In fact, the most pronounced results on site-specific RNA cleavage by imidazole-containing oligonucleotide conjugates have been obtained using this particular tRNA–yeast $tRNA^{Phe}$ (15–17,31,32).

The investigated conjugates exhibit similar cleaving activities. Under the most discriminating concentration of the conjugates (1 μM), twice that of $tRNA^{Phe}$, conjugates B-R(1/1), B-R(1/2) and B-R(2) cleaved 50, 30 and 28% of RNA after 4 h incubation, respectively. These data indicate that conjugates display higher activity when the cyclohexyl moiety is used as an anchor group. Surprisingly, conjugate B-R(1/1) with the shorter linker was more active than B-R(1/2). Molecular modelling data suggest that the advantage in reaching the target site provided by a longer linker in the H-R(1/2) molecule is diminished by an increased conformational freedom of the cleaving groups.

The conjugates under study display similar cleavage specificities: the major cleavage site was phosphodiester bond C_{63}–A_{64}; the adjacent bond (A_{64}–G_{65}) was cleaved at a lower rate. No cleavage at C_{61}–A_{62} was observed. Molecular modelling data provide a reasonable explanation of the absence of cleavage at C_{61}–A_{62}. It appears to be necessary to overcome a very high-energy barrier to position the cleaving constructs near the C_{61}–A_{62} potential cleavage site (∼3 Å). The reason for this seems to be marked steric hindrance at the C_{61}–A_{62} potential cleavage site, which seems to be highly structured due to its involvement in stacking interactions with the adjacent heteroduplex. This agrees with the fact that the conformations O-R(n)$_{61–62}$ obtained are energetically less favourable than the O-R(n)$_{63–64}$ conformations (see Table 1), suggesting a lower probability for cleaving groups to attack the C_{61}–A_{62} site.

Surprisingly, the conjugates under study cleaved the A_{64}–G_{65} phosphodiester bond with notable efficiency. It is known that phosphodiester bonds within 5′Pu–Pu3′ sequences are quite resistant to cleavage. However, this particular bond (A_{64}–G_{65}) was shown to be cleaved by imidazole-containing small ribonuclease mimics (9,26,27). The reduced cleavage efficiency at the A_{64}–G_{65}, compared with C_{63}–A_{64}, can be explained by both inferior cleavage sensitivity and the more distant location of this site from the cleaving groups.

Molecular modelling is consistent with the experimental observations and equally provides confidence in the ability to use such methods to improve the molecular design. The results of molecular modelling indicate the high conformational flexibility of the cleaving constructs. No particular stable contacts between hydrolytic groups and the RNA chain were detected, implying the absence of any pre-scaffolded conformation(s). Thus, the cleavage of the phosphodiester bond seems to be a random event, happening every time correctly oriented catalytic groups come close to the

cleavage site. Although the probability and life time(s) of favourable ('in') conformation(s) are restricted, cleavage occurs at reasonable rates. Therefore, the rate of the *cleavage event itself* is likely to be high and restricted at this stage by non-perfect structural parameters for cleaving constructs. Further improvement should be possible by rational design of the catalytic structures of the conjugates.

SUPPLEMENTARY MATERIAL

Supplementary Material is available at NAR Online.

ACKNOWLEDGEMENTS

This work was supported by the grants from The Welcome Trust (no. 063630), CRDF NO-008-X1, RFBR no. 02-04-48664 and 03-04-06238, SS-1384.2003.4, RAS program 'Molecular and cellular biology', and SB RAS for Interdisciplinary investigations N50 and in Support of young scientists.

REFERENCES

1. Stern,M.K., Bashkin,J.K. and Sall,E.D. (1990) Hydrolysis of RNA by transition metal complexes. *J. Am. Chem. Soc*., **112**, 5357–5359.
2. Barbier,B. and Brack,A. (1987) Search for catalytic properties of simple polypeptides. *Orig. Life Evol. Biosph*., **17**, 381–390.
3. Li,Y., Zhao,Y., Hatfield,S., Wan,R., Zhu,Q., Li,X., McMills,M., Ma,Y., Li,J., Brown,K.L., He,C., Liu,F. and Chen,X. (2000) Dipeptide seryl-histidine and related oligopeptides cleave DNA, protein and carboxyl ester. *Bioorg. Med. Chem*., **8**, 2675–2680.
4. Michaelis,K. and Kalesse,M. (1999) Selective cleavage of the HIV-1 TAR–RNA with a peptide-cyclen conjugate. *Angew. Chem. Int. Ed. Engl*., **38**, 2243–2245.
5. Yoschinari,K., Yamazaki,K. and Komiyama,M. (1991) Oligoamines as a simple and efficient catalysts. *J. Am. Chem. Soc*., **113**, 5899–5901.
6. Keck,M.V. and Hecht,S.M. (1995) Sequence-specific hydrolysis of yeast $tRNA^{(Phe)}$ mediated by metal-free bleomycin. *Biochemistry*, **34**, 12029–12037.
7. Podyminogin,M.A., Vlassov,V.V. and Giege,R. (1993) Synthetic RNA-cleaving molecules mimicking ribonuclease A active center. Design and cleavage of tRNA transcripts. *Nucleic Acids Res*., **21**, 5950–5956.
8. Vlassov,V.V., Zuber,G., Felden,B., Behr,J. and Giege,R. (1995) Cleavage of tRNA with imidazole and spermine imidazole constructs: a new approach for probing RNA structure. *Nucleic Acids Res*., **23**, 3161–3167.
9. Konevetz,D.A., Beck,I.A., Beloglazova,N.G., Sulimenkov,I.V., Sil'nikov,V.N., Zenkova,M.A., Shishkin,G.V. and Vlassov,V.V. (1999) Artificial ribonucleases: synthesis and RNA cleaving properties of cationic conjugates bearing imidazole residues. *Tetrahedron*, **55**, 503–514.
10. Komiyama,M. and Inokava,T. (1994) Selective hydrolysis of tRNA by ethylenediamine bound to a DNA oligomer. *J. Biochem*., **116**, 719–720.
11. Hovinen,J., Guzaev,A., Azhayeva,E., Azhaev,A. and Lönberg,H. (1995) Imidazole tethered oligodeoxyribonucleotides: synthesis and RNA cleaving activity. *J. Org. Chem*., **60**, 2205–2209.
12. Silnikov,V.N., Zuber,G., Behr,J.-P., Giege,R. and Vlassov,V.V. (1996) Design of ribonuclease mimics for sequence specific cleavage of RNA. *Phosphor Sulfur Silicon*, **109–110**, 277–280.
13. Hall,J., Husken,D. and Häner,R. (1996) Towards artificial ribonucleases: the sequence-specific cleavage of RNA in a duplex. *Nucleic Acids Res*., **24**, 3522–3526.
14. Pyshnyi,D., Repkova,M., Lokhov,S., Ivanova,E., Venyaminova,A. and Zarytova,V.D. (1997) Oligonucleotide-peptide conjugates for RNA cleavage. *Nucleosides Nucleotides*, **16**, 1571–1574.
15. Yurchenko,L., Silnikov,V., Godovikova,T., Shishkin,G., Toulme,J.-J. and Vlassov,V. (1997) Cleavage of Leishmania mini-exon sequence by oligonucleotides conjugated to a diimidazole construction. *Nucleosides Nucleotides*, **16**, 1741–1745.
16. Vlassov,V., Abramova,T., Giege,R. and Silnikov,V. (1997) Sequence-specific cleavage of yeast $tRNA^{Phe}$ with oligonucleotides conjugated to a diimidazole construct. *Antisense Nucleic Acid Drug Dev*., **7**, 39–42.
17. Ushijima,K. and Takaku,H. (1998) Site-specific cleavage of tRNA by imidazole and/or primary amine groups bound at the 5′-end of oligodeoxyribonucleotides. *Biochim. Biophys. Acta*, **1379**, 217–223.
18. Huber,P.W. (1993) Chemical nucleases: their use in studying RNA structure and RNA–protein interactions. *FASEB J*., **7**, 1367–1375.
19. Uhlmann,E. and Peymann,A. (1990) Antisense oligonucleotides: a new therapeutic principle. *Chem. Rev*., **90**, 544–584.
20. Trawick,B.N., Daniher,A.T. and Bashkin,J.K. (1998) Inorganic mimics of ribonucleases and ribozymes: from random cleavage to sequence-specific chemistry to catalytic antisense drugs. *Chem. Rev*., **98**, 939–960.
21. Komiyama,M. and Sumaoka,J. (1998) Progress towards synthetic enzymes for phosphoester hydrolysis. *Curr. Opin. Chem. Biol*., **2**, 751–757.
22. Matsumura,K., Endo,M. and Komyiama,M. (1994) Lanthanide complex-oligo-DNA hybrid for sequence-selective hydrolysis of RNA. *J. Chem. Soc. Chem. Commun*., 2019–2020.
23. Magda,D., Miller,R.A., Sessler,J.L. and Iverson,B.L. (1994) Site-specific hydrolysis of RNA by Europium(III) texaphyrin conjugated to a synthetic oligodeoxyribonucleotide. *J. Am. Chem. Soc*., **116**, 7439–7440.
24. Häner,R., Hall,J., Pfützer,A. and Hüsken,D. (1998) Development of artificial ribonucleases. *Pure Appl. Chem*., **70**, 111–116.
25. Canaple,L., Husken,D. and Haner,R. (2002) Artificial ribonucleases: efficient and specific *in vitro* cleavage of human *c-raf-1* RNA. *Bioconjug. Chem*., **13**, 945–951.
26. Giege,R., Felden,B., Sil'nikov,V.N., Zenkova,M.A. and Vlassov,V.V. (2000) Cleavage of RNA with synthetic ribonuclease mimics. *Methods Enzymol*., **318**, 147–165.
27. Zenkova,M.A., Sil'nikov,V.N., Beloglazova,N.G., Giege,R. and Vlassov,V.V. (2001) RNA cleavage by 1,4-diazabicyclo[2.2.2]octane-imidazole conjugates. *Methods Enzymol*., **341**, 468–490.
28. Zhdan,N.S., Kuznetsova,I.L., Zenkova,M.A., Vlassov,A.V., Silnikov,V.N., Giege,R. and Vlassov,V.V. (1999) Synthesis and characterization of artificial ribonucleases. *Nucleosides Nucleotides*, **18**, 1491–1492.
29. Komiyama,M., Inokava,T. and Yoshinari,K. (1995) Ethylendiamine-oligo DNA hybrid as sequence-selective artificial ribonuclease. *J. Chem. Soc. Chem. Commun*., 1647–1652.
30. Bashkin,J.K., Frolova,E.I. and Sampath,U. (1994) Sequence-specific cleavage of HIV mRNA by a ribozyme mimic. *J. Am. Chem. Soc*., **116**, 5981–5982.
31. Beloglazova,N.G., Sil'nikov,V.N., Zenkova,M.A. and Vlassov,V.V. (2000) Cleavage of yeast $tRNA^{Phe}$ with complementary oligonucleotide conjugated to a small ribonuclease mimic. *FEBS Lett*., **481**, 277–280.
32. Reynolds,M.A., Beck,T.A. and Arnold,L.J. (1996) Antisense oligonucleotide containing an internal, non-nucleotide-based linker promote site-specific cleavage of RNA. *Nucleic Acids Res*., **24**, 760–765.
33. Polushin,N.N. (2000) The precursor strategy: terminus methoxyoxalamido modifiers for single and multiple functionalization of oligodeoxyribonucleotides. *Nucleic Acids Res*., **28**, 3125–3133.
34. Polushin,N.N., Morocho,A.M., Chen,B.C. and Cohen,J.S. (1994) Synthesis and characterization of imidazoyl-linked synthons and 3′-conjugated thymidine derivatives. *Nucleic Acids Res*., **22**, 639–645.
35. Petyuk,V.A., Zenkova,M.A., Giege,R. and Vlassov,V.V. (2000) Mechanism of oligonucleotide hybridization with the 3′-terminal region of yeast tRNA(Phe). *Mol. Biol. (Moskow)*, **34**, 879–886.
36. Petyuk,V., Zenkova,M., Giege,R. and Vlassov,V. (1999) Hybridization of antisense oligonucleotides with the 3′-part of $tRNA^{Phe}$. *FEBS Lett*., **444**, 217–221.
37. Vlassov,A.V., Vlassov,V.V. and Giege,R. (1996) RNA hydrolysis catalyzed by imidazole as a reaction for studying the secondary structure of RNA and complexes of RNA with oligonucleotides. *Dokl. Akad. Nauk*., **349**, 411–413.
38. Nishikawa,S., Morioka,H., Kim,H.J., Fuchimura,K., Tanaka,T., Uesugi,S., Hakoshima,T., Tomita,K., Ohtsuka,E. and Ikehara,H. (1987) Two histidine residues are essential for ribonuclease T1 activity as is the case for ribonuclease A. *Biochemistry*, **26**, 8620–8624.
39. Stewart,J.P. (1990) MOPAC: a semi-empirical molecular orbital program. *J. Comput. Aided Mol. Des*., **4**, 1–105.

40. Breslow,R., Dong,S.D., Webb,Y. and Xu,R. (1996) Further studies on the buffer-catalyzed cleavage and isomerization of uridyluridine medium and ionic strength effect on catalysis by morpholine, imidazole, and acetate buffers help clarify the mechanisms involved and their relationship to the mechanism used by the enzyme ribonuclease and by a ribonuclease mimic. *J. Am. Chem. Soc.*, **118**, 6588–6600.
41. Fontecilla-Camps,J.C., de Llorens,R., le Du,M.H. and Cuchillo,C.M. (1994) Crystal structure of ribonuclease A·d(ApTpApApG) complex. Direct evidence for extended substrate recognition. *J. Biol. Chem.*, **269**, 21526–21531.
42. Birdsall,D.L. and McPherson,A. (1992) Crystal structure disposition of thymidylic acid tetramer in complex with ribonuclease A. *J. Biol. Chem.*, **267**, 22230–22236.
43. Wlodawer,A., Miller,M. and Sjolin,L. (1983) Active-site of RNase—neutron-diffraction study of a complex with uridine vanadate, a transition-state analog. *Proc. Natl Acad. Sci. USA*, **80**, 3628–3631.
44. Vitagliano,L., Merlino,A., Zagari,A. and Mazzarella,L. (2000) Productive and non-productive binding of ribonucleases A: X-ray structure of two complexes with uridylyl(2′,5′)guanosine. *Protein Sci.*, **9**, 1217–1225.
45. Polushin,N.N. (1996) Synthesis of functionally modified oligonucleotides from methoxyoxalamido precursors. *Tetrahedron Lett.*, **37**, 3231–3234.
46. Kumazawa,Y., Yokogawa,T., Tsurui,H., Miura,K. and Watanabe,K. (1994) Effect of the higher-order structure of tRNAs on the stability of hybrids with oligodeoxyribonucleotides: separation of tRNA by an efficient solution hybridization. *Nucleic Acids Res.*, **20**, 2223–2232.
47. Zenkova,M.A., Petyuk,V.A., Giege,R. and Vlassov,V.V. (1998) Interaction of complementary oligonucleotides with the 3′-end of yeast $tRNA^{Phe}$. *Dokl. Akad. Nauk.*, **361**, 260–263.
48. Petyuk,V., Serikov,R., Tolstikov,V., Potapov,V., Giege,R., Zenkova,M. and Vlassov,V. (2000) Invasion of strongly binding oligonucleotides into tRNA structure. *Nucleosides Nucleotides Nucleic Acids*, **19**, 1145–1158.
49. Serikov,R.N., Petyuk,V.N., Vlassov,V.V. and Zenkova,M.A. (2002) Hybridization of antisense oligonucleotides with yeast $tRNA^{Phe}$: factors determining the efficiency of interaction. *Russ. Chem. Bull. Int. Ed.*, **51**, 1156–1165.
50. Romby,P., Moras,D., Dumas,P., Ebel,J.-P. and Giege,R. (1987) Comparison of the tertiary structure of yeast tRNA(Asp) and tRNA(Phe) in solution. *J. Mol. Biol.*, **195**, 193–204.
51. Kim,S.H., Suddath,F.L., Quigley,G.J., McPherson,A., Sussman,J.L., Wang,A.H., Seeman,N.C. and Rich,A. (1974) Three-dimensional tertiary structure of yeast phenylalanine transfer RNA. *Science*, **185**, 435–440.
52. Vlassov,V.V., Sil'nikov,V.N. and Zenkova,M.A. (1998) Chemical ribonucleases. *Mol. Biol. (Moskow)*, **32**, 62–70.
53. Santoro,S.W. and Joyce,G.F. (1998) Mechanism and stability of an RNA-cleaving DNA-enzyme. *Biochemistry*, **37**, 13330–13342.
54. Joyce,G.F. (2001) RNA cleavage by 10–23 DNA enzyme. *Methods Enzymol.*, **341**, 503–517.
55. Craig,M.E., Crothers,D.M. and Doty,P. (1971) Relaxation kinetics of dimer formation by self complementary oligonucleotides. *J. Mol. Biol.*, **62**, 383–401.
56. Homann,M., Rittner,K. and Sczakiel,G. (1993) Complementary large loops determine the rate of RNA duplex formation *in vitro* in the case of an effective antisense RNA directed against the human immunodeficiency virus type 1. *J. Mol. Biol.*, **233**, 7–15.
57. Tomizawa,J. (1990) Control of ColE1 plasmid replication. Intermediates in the binding of RNA I and RNA II. *J. Mol. Biol.*, **212**, 683–694.
58. Kittle,J.D., Simons,R.W., Lee,J. and Kleckner,N. (1989) Insertion sequence IS10 anti-sense pairing initiates by an interaction between the 5′ end of the target RNA and a loop in the anti-sense RNA. *J. Mol. Biol.*, **210**, 561–572.
59. Misra,V.K. and Draper,D.E. (2002) The linkage between magnesium ions and RNA folding. *J. Mol. Biol.*, **317**, 507–521.
60. Choi,B.S. and Redfield,A.G. (1995) Proton-exchange and base pair kinetics of yeast $tRNA^{phe}$ and $tRNA^{Asp1}$. *J. Biochem.*, **117**, 515–520.
61. Friedrich,M.W. and Hagerman,P.J. (1997) Conformational transitions of an unmodified tRNA: implications for RNA folding. *Biochemistry*, **37**, 16349–16359.
62. Barone,F., Cellai,L., Matzeu,M., Mazzei,F. and Pedone,F. (2000) DNA, RNA and hybrid RNA–DNA oligomers of identical sequence: structural and dynamic differences. *Biophys. Chem.*, **86**, 37–47.
63. Xiong,Y. and Sundaralingam,M. (2000) Crystal structure of a DNA–RNA hybrid duplex with a polypurine RNA r(GAAGAAGAG) and a complementary polypyrimidine DNA d(CTCTTCTTC). *Nucleic Acids Res.*, **28**, 2171–2176.
64. Hantz,E., Larue,V., Ladam,P., Le Moyec,L., Gouyette,C. and Dinh,T.H. (2001) Solution conformation of an RNA–DNA hybrid duplex containing a pyrimidine RNA strand and a purine DNA strand. *Int. J. Biol. Macromol.*, **28**, 273–284.
65. Zegers,I., Maes,D., Daothi,H., Poortmans,F., Palmer,R. and Wyns,L. (1994) The structures of RNase-A complexed with 3′-CMP and d(CpA)—active-site conformation and conserved water-molecules. *Protein Sci.*, **3**, 2322–2339.
66. Aguilar,C.F., Thomas,P.J., Moss,D.S., Mills,A. and Palmer,R.A. (1991) Novel non-productively bound ribonuclease inhibitor complexes—high-resolution X-ray refinement studies on the binding of RNase-A to cytidylyl-2′,5′-guanosine (2′,5′CpG) and deoxycytidylyl-3′,5′-guanosine (3′,5′dCpdG). *Biochim. Biophys. Acta*, **1118**, 6–20.
67. Aguilar,C.F., Thomas,P.J., Mills,A., Moss,D.S. and Palmer,R.A. (1992) Newly observed binding mode in pancreatic ribonuclease. *J. Mol. Biol.*, **224**, 265–267.
68. Endo,M., Azuma,Y., Saga,Y., Kuzuya,A., Kawai,G. and Komiyama,M. (1997) Molecular design for a pinpoint RNA scission. Interposition of oligoamines between two DNA oligomers.1. *J. Org. Chem.*, **62**, 846–852.
69. Verheijen,J.C., Deiman,B.A.L.M., Yeheskiely,E., van der Marel,G.A. and van Boom,J.H. (2000) Efficient hydrolysis of RNA by a PNA-diethylentriamine adduct. *Angew. Chem. Int. Ed.*, **39**, 369–371.